Avoided intersections of nodal lines

Alejandro G Monastra[1], Uzy Smilansky[1] and Sven Gnutzmann[2]

[1] Department of Physics of Complex Systems, The Weizmann Institute of Science, Rehovot 76100, Israel
[2] Institute for Theoretical Physics, Freie Universität Berlin, 14195 Berlin, Germany

Abstract
We consider real eigenfunctions of the Schrödinger operator in 2D. The nodal lines of separable systems form a regular grid, and the number of nodal crossings equals the number of nodal domains. In contrast, for wavefunctions of non-integrable systems nodal intersections are rare, and for random waves, the expected number of intersections in any finite area vanishes. However, nodal lines display characteristic avoided crossings which we study in this work. We define a measure for the avoidance range and compute its distribution for the random wave ensemble. We show that the avoidance range distribution of wavefunctions of chaotic systems follows the expected random wave distributions, whereas for wavefunctions of classically integrable but quantum non-separable systems, the distribution is quite different. Thus, the study of the avoidance distribution provides more support to the conjecture that nodal structures of chaotic systems are reproduced by the predictions of the random wave ensemble.

PACS numbers: 05.45.Mt, 02.10.Yn

1. Introduction

The morphology of the nodal sets of wavefunctions depends crucially on whether the underlying classical dynamics is integrable or chaotic. This was first proposed in [1] and was followed by the study of various features of the nodal lines, such as the distribution of its curvatures [2]. Recently, the counting statistics of nodal domains for integrable and chaotic systems were investigated in [3], and it was shown that in the chaotic case, the statistics follow the predictions derived by assuming that the wavefunctions are random superpositions of plane waves [4, 5]. Local effects due to boundary conditions, and the corresponding modifications of the random wave ensembles were also studied [6, 7].

The interest in the properties of the nodal set is not confined to the physics literature only. Most of the mathematics literature on this subject is concerned with solutions of the Helmholtz equation in the interior of compact domains in $\mathbb{R}^2$ with Dirichlet or Neumann
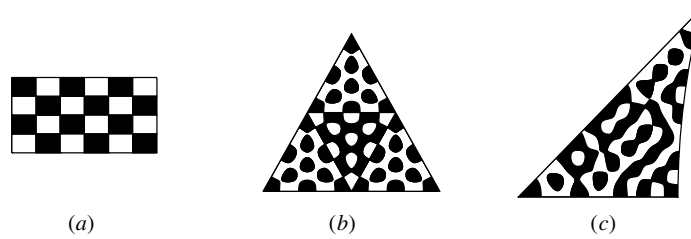
Figure 1. Eigenfunctions of 2D billiards: (*a*) rectangle (separable dynamics); (*b*) equilateral triangle (integrable, non-separable dynamics); (*c*) Sinai (chaotic dynamics).

boundary conditions. Courant [8] and later Pleijel [9] pioneered these studies, and computed an upper bound on the number of nodal domains. Krahn [10] provided a lower bound for the area of a nodal domain. Other authors gave estimates on, e.g., the length of the nodal sets [11], and addressed the general properties of the nodal network [12].

Uhlenbeck's theorem [13] states that the nodal lines of 'generic' wavefunctions do not intersect (this statement will be further discussed in the next section). An important class of exceptions to this rule are the eigenfunctions of separable systems, where the nodal lines form a grid, and the number of intersections equals the number of nodal domains. The purpose of this work is to provide a *quantitative measure* of the degree by which nodal lines avoid each other. We shall associate the *avoidance range* with each avoided crossing, and will compute their distribution for the random wave ensemble. The avoidance range vanishes for an intersection, and therefore, the avoidance range distribution for separable functions is proportional to a Dirac δ at zero. We also show that eigenfunctions of classically chaotic systems display an avoidance range distribution which is similar to that obtained for a random wave ensemble, while for an intermediate system, the avoidance distribution differs substantially from either of the extreme distributions mentioned above. The nodal structure for a few representative wavefunctions can be seen in figure 1. The wavefunction of a rectangle (*a*) displays a perpendicular grid of nodal lines typical of separable systems. An equilateral triangle (*b*) is classically integrable, but not separable, and the wavefunction shows a few crossings and avoided crossings of the nodal lines. The domain in (*c*) is a Sinai billiard where the classical dynamics is chaotic. With the exception of the boundary crossings, the nodal set displays a characteristic set of avoided crossings.

The paper is organized as follows. We shall begin the next section by discussing the nodal structure of general solutions of the Helmholtz equation. We shall then identify avoided crossings of the nodal lines, and define the corresponding avoidance range. The avoidance range distribution will be written down explicitly. In section 3, we shall define the random wave ensemble and compute explicitly the expected distribution of the avoidance ranges. The resulting expression will be compared with the avoidance distributions obtained numerically for high lying eigenfunctions of a chaotic domain. For Dirichlet problems, the boundary belongs to the nodal set, where nodal intersections occur at a density which is approximately two intersections per wavelength. This property cannot be reproduced by the uniform random wave ensembles, which are expected to account for bulk properties. This problem, in the context of the avoided crossing distribution, is discussed at the end of section 3.

2. Avoided crossings of nodal lines and the avoidance range

We consider real solutions of the Helmholtz equation in a domain $\Omega \in \mathbb{R}^2$ which can be expressed as linear superpositions of regular solutions of the equation in the entire plane. They

can be expressed in terms of either plane or cylindrical waves, and the two representations are equivalent. In the plane wave representation the wavefunction is written as

$$\Psi(\mathbf{r}) = \sum_{n=-\infty}^{\infty} a_n \, e^{i\mathbf{k}_n \cdot \mathbf{r}} \tag{1}$$

with wave vectors ($\mathbf{k}_n = -\mathbf{k}_{-n}$, $|\mathbf{k}_n|^2 = k^2$) directed at an angle θ_n and coefficients which ensure that the series (1) converges absolutely (we require $a_n^* = a_{-n}$ to render $\Psi(\mathbf{r})$ real). Using the expansion of a plane wave in cylindrical coordinates we get

$$\Psi(\mathbf{r}) = \sum_{l=-\infty}^{\infty} \alpha_l J_l(kr) \, e^{il\theta} \tag{2}$$

with

$$\alpha_l = \sum_{n=-\infty}^{\infty} a_n \, e^{il\theta_n} \qquad \text{and} \qquad \alpha_l^* = (-1)^l \alpha_{-l}. \tag{3}$$

The infinite sums in both (1) and (2) can be truncated, when one considers domains of finite area. Semiclassical arguments show that the necessary number of terms is $L \approx \mathcal{L}k/\pi$, where $\mathcal{L}$ is the perimeter of the domain. For reasons which will become clear in the following, we prefer to use the cylindrical wave representation in this work.

The expansion (2) refers to a particular choice of the origin. Using Graf's addition theorem [14] the origin can be shifted to $\mathbf{r}$, and the wavefunction retains its form,

$$\Psi(\mathbf{r} + \rho) = \sum_m \alpha_m(\mathbf{r}) J_m(k\rho) \, e^{im\phi} \tag{4}$$

where

$$\alpha_m(\mathbf{r}) = \sum_l \alpha_l(\mathbf{0}) J_{l-m}(kr) \, e^{il\theta} \tag{5}$$

with $\alpha_l(\mathbf{0}) = \alpha_l$, and the angle ϕ is measured from the direction defined by $\mathbf{r}$. The translated coefficients $\alpha_m(\mathbf{r}) = \beta_m(\mathbf{r}) + i\gamma_m(\mathbf{r})$ are related to the wavefunction and its derivatives computed at the point $\mathbf{r}$:

$$\beta_0(\mathbf{r}) = \Psi(\mathbf{r})$$

$$\beta_1(\mathbf{r}) = \frac{1}{k}\Psi_r(\mathbf{r}) \qquad\qquad \gamma_1(\mathbf{r}) = -\frac{1}{kr}\Psi_\theta(\mathbf{r})$$

$$\beta_2(\mathbf{r}) = \Psi(\mathbf{r}) + \frac{2}{k^2}\Psi_{rr}(\mathbf{r}) \qquad \gamma_2(\mathbf{r}) = \frac{2}{k^2r^2}(\Psi_\theta(\mathbf{r}) - r\Psi_{r\theta}(\mathbf{r})) \tag{6}$$

$$\Psi_{\theta\theta}(\mathbf{r}) = -kr\beta_1(\mathbf{r}) - \frac{k^2r^2}{2}(\beta_2(\mathbf{r}) + \beta_0(\mathbf{r})).$$

In the close vicinity of $\mathbf{r}$, where $k\rho < 1$, and to second order in $k\rho$

$$\Psi(\mathbf{r} + \rho) \approx \beta_0(\mathbf{r}) \left(1 - \left(\frac{k\rho}{2}\right)^2\right) + |\alpha_1(\mathbf{r})| \left(\frac{k\rho}{2}\right) \cos(\phi + \phi_1)$$

$$+ \frac{1}{2}|\alpha_2(\mathbf{r})| \left(\frac{k\rho}{2}\right)^2 \cos 2(\phi + \phi_2) \tag{7}$$

where ϕ_l are the phases of $\alpha_l(\mathbf{r})$. If $\beta_0(\mathbf{r}) = 0$, $\mathbf{r}$ is a nodal point. It cannot be an isolated zero since the second term vanishes on the line segment through $\mathbf{r}$ which is oriented along the direction $\frac{\pi}{2} - \phi_1$. Hence, the nodal set consists of lines. Two nodal lines intersect at $\mathbf{r}$

if both $\beta_0(\mathbf{r}) = 0$ and $\alpha_1(\mathbf{r}) = 0$, while $\alpha_2(\mathbf{r}) \neq 0$. The intersection is perpendicular since $\cos 2(\phi + \phi_2)$ vanishes along two perpendicular lines which intersect at $\mathbf{r}$. For the time being we shall continue the discussion assuming that $\alpha_2(\mathbf{r}) \neq 0$. The more general case will be commented on at the end of this section.

An *avoided crossing* occurs at $\mathbf{r}$ when $\alpha_1(\mathbf{r}) = 0$ and $|\alpha_2(\mathbf{r})| > |\beta_0(\mathbf{r})| > 0$. In other words, when $\mathbf{r}$ is a *saddle point* of the wavefunction. This can be easily seen by writing the equation of the zero set of (7) in terms of the local coordinates $\rho = (\xi, \eta)$,

$$1 = \xi^2 \left(\frac{\beta_0(\mathbf{r}) - |\alpha_2(\mathbf{r})|}{\beta_0(\mathbf{r})} \right) + \eta^2 \left(\frac{\beta_0(\mathbf{r}) + |\alpha_2(\mathbf{r})|}{\beta_0(\mathbf{r})} \right). \tag{8}$$

This is a hyperbola (ellipse) if $|\alpha_2(\mathbf{r})|$ is larger (smaller) than $|\beta_0(\mathbf{r})|$. At an avoided crossing, the scaled distance between the two branches is

$$z(\mathbf{r}) \equiv kd(\mathbf{r}) = 4 \sqrt{\frac{|\beta_0(\mathbf{r})|}{|\beta_0(\mathbf{r})| + |\alpha_2(\mathbf{r})|}}. \tag{9}$$

This is the *avoidance range* associated with the avoided crossing at $\mathbf{r}$.

A few comments are in order:

(i) At a nodal intersection $z = 0$.

(ii) At a saddle point $|\alpha_2(\mathbf{r})| > |\beta_0(\mathbf{r})|$, hence $z < 2\sqrt{2}$.

(iii) An equivalent expression for $z(\mathbf{r})$ in terms of $\Psi(\mathbf{r})$ and its Cartesian derivatives reads

$$z(\mathbf{r}) = 4 \sqrt{\left. \frac{k^2 |\Psi|}{k^2 |\Psi| + \sqrt{4\Psi_{xy}^2 + (\Psi_{xx} - \Psi_{yy})^2}} \right|_{\mathbf{r}}}. \tag{10}$$

(iv) Consider an elliptic critical point of the wavefunction. In the quadratic approximation the area of the elliptic nodal domain is

$$\mathcal{A} = 4\pi k^{-2} \sqrt{\left. \frac{\beta_0^2}{\beta_0^2 - |\alpha_2|^2} \right|_{\mathbf{r}}}. \tag{11}$$

This area is always larger than $4\pi k^{-2}$. Krahn's theorem [10] gives $j_{0,1}^2 \pi k^{-2}$ as the maximal lower bound to the area of any nodal domain, where $j_{0,1} \approx 2.405$ is the first zero of the Bessel function $J_0(x)$. The lower bound $4\pi k^{-2}$ is smaller but not very far from Krahn's exact value and thus consistent.

So far we considered the intersections of two nodal lines. However, higher order intersections may occur. In general, if the first non-vanishing coefficient at $\mathbf{r}$ is α_q, then $\mathbf{r}$ is a nodal point of order q, where q nodal lines intersect at angles $\frac{\pi}{q}$. The higher the q, the rarer are the intersections, since more conditions are to be satisfied by the coefficients. This explains the Uhlenbeck's theorem [13] mentioned above. From now on we shall discuss the most common intersections with $q = 2$, and comment on the higher order intersections whenever necessary.

Up to now we discussed individual avoided crossings, and defined the associated avoidance ranges. In the following section, we shall consider the distribution of the avoidance ranges of a wavefunction in the domain of its definition, and compute its mean for random wave ensembles.

3. Avoidance range distributions

The number of the critical points of $\Psi(\mathbf{r})$ in the domain Ω is given by

$$N_C = \int_\Omega r \, \mathrm{d}r \, \mathrm{d}\theta \, \delta(\Psi_r(\mathbf{r})) \delta\left(\frac{1}{r}\Psi_\theta(\mathbf{r})\right) |\mathcal{J}(\mathbf{r})| \tag{12}$$

with $\mathcal{J}(\mathbf{r}) = \frac{1}{r}\left(\Psi_{rr}(\mathbf{r})\Psi_{\theta\theta}(\mathbf{r}) - \Psi_{r\theta}^2(\mathbf{r})\right)$ being the Jacobian. Using (7) we get

$$N_C = \frac{k^2}{4} \int_\Omega r \, \mathrm{d}r \, \mathrm{d}\theta \, \delta(\beta_1(\mathbf{r})) \delta(\gamma_1(\mathbf{r})) \big||\alpha_2(\mathbf{r})|^2 - \beta_0^2(\mathbf{r})\big|. \tag{13}$$

To count the saddle points, we add the restriction $|\alpha_2(\mathbf{r})|^2 - \beta_0^2(\mathbf{r}) > 0$ and obtain

$$N_S = \frac{k^2}{4} \int_\Omega r \, \mathrm{d}r \, \mathrm{d}\theta \, \delta(\beta_1(\mathbf{r})) \delta(\gamma_1(\mathbf{r})) \big(|\alpha_2(\mathbf{r})|^2 - \beta_0^2(\mathbf{r})\big) \Theta\big(|\alpha_2(\mathbf{r})|^2 - \beta_0^2(\mathbf{r})\big). \tag{14}$$

Combining (14) and (9), the number of avoided crossings with avoidance ranges less than z is

$$\tilde{\mathcal{I}}(z) = \frac{k^2}{4} \int_\Omega r \, \mathrm{d}r \, \mathrm{d}\theta \, \delta(\beta_1(\mathbf{r})) \delta(\gamma_1(\mathbf{r})) \big(|\alpha_2(\mathbf{r})|^2 - \beta_0^2(\mathbf{r})\big) \Theta\big(|\alpha_2(\mathbf{r})|^2 - \beta_0^2(\mathbf{r})\big) \Theta(z - z(\mathbf{r}))$$
$$\tag{15}$$

and the fraction of the total number is $\mathcal{I}(z) = \tilde{\mathcal{I}}(z)/N_S$. This counting function, and its associated density $\mathcal{P}(z) \equiv \frac{\mathrm{d}\mathcal{I}(z)}{\mathrm{d}z}$ are the distributions which characterize the avoided crossings of the nodal set. The range of z is $[0, 2\sqrt{2}]$. $\mathcal{I}(z)$ is normalized such that it takes the value 1 at $z = 2\sqrt{2}$. One can easily check that an avoided crossing of order q is counted in (15) with a multiplicity $q - 1$. The number (including multiplicity) of nodal crossings provides the value of $\mathcal{I}(0)$. The effective multiplicity of nodal crossings of the boundary is reduced by a factor of one half.

Numerically computed $\mathcal{I}(z)$ are shown in figure 2 for the three wavefunctions plotted in figure 1. The computed $\mathcal{I}(z)$ do not take into account the nodal crossings of the boundary. For the separable billiard all the saddle points have zero avoidance range, and the function $\mathcal{I}(z)$ is trivially equal to 1 in all the z range. In the triangular billiard there are still some saddle points with zero avoidance range (nodal crossings), but most of them have a finite avoidance range. For the chaotic billiard, all the calculated saddle points have a finite avoidance range.

3.1. Avoidance range distribution for the random wave ensemble

One of the main goals of this work is to show that the properties of the nodal set of chaotic billiards, as detected by the distribution of avoidance ranges, are reproduced by the distributions computed for the random wave ensembles. Because wavefunctions are subject to boundary conditions, it is expected that the predictions of the isotropic random wave ensemble used e.g. in [3, 5], are relevant only to the bulk of the domain, and will do poorly in the $\lambda = \left(\frac{2\pi}{k}\right)$ vicinity of the boundary. This was observed and discussed in [3].

The isotropic random wave ensemble is the ensemble of wavefunctions (2) where the real parameters β_l and γ_l are independent identically distributed random Gaussian variables with zero mean and unit variance for all $|l| \geqslant 1$. Because $\gamma_0 = 0$ the variance of β_0 is twice that of all the others. The ensemble average of a function f will be denoted by $\langle f \rangle$. The local coefficients $\alpha_l(\mathbf{r}) = \beta_l(\mathbf{r}) + i\gamma_l(\mathbf{r})$ were derived from the original ones by a unitary transformation. Hence, they are also independent identically distributed Gaussian variables, and the ensemble averages of the number of critical points (12), the number of saddle points (14) and the mean distribution of avoidance ranges (15) can be computed by considering
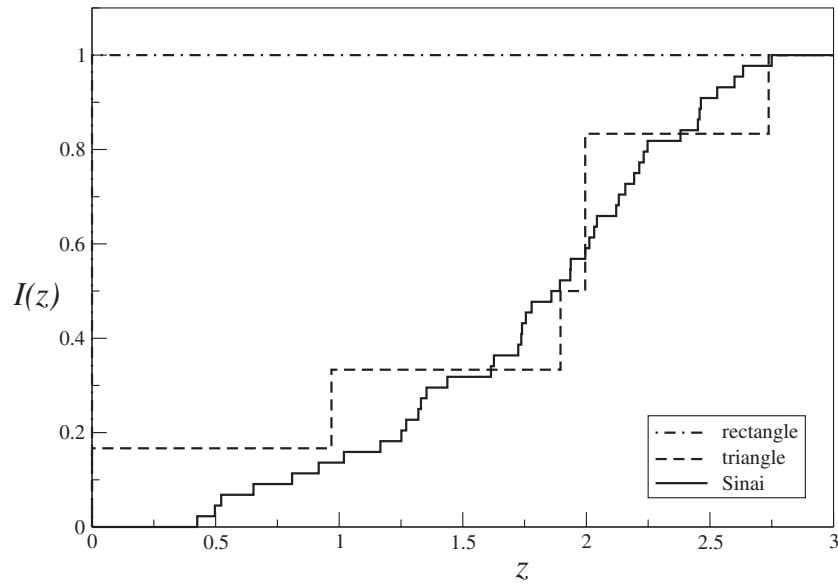
Figure 2. Normalized cumulative histograms of the avoidance ranges $\mathcal{I}(z)$ for the three wavefunctions plotted in figure 1: rectangle (dash-point line); triangle (dashed line); Sinai (full line).

Gaussian integrations with respect to the variables β_0, β_1, γ_1, β_2 and γ_2. A straightforward integration gives

$$\langle N_C \rangle = \frac{k^2 |\Omega|}{2\pi \sqrt{3}} \qquad \langle N_S \rangle = \frac{k^2 |\Omega|}{4\pi \sqrt{3}} \tag{16}$$

where $|\Omega|$ is the area of the domain. The average number of saddle points is a half of the number of critical points. The other half are the points where the wavefunction has either a minimum or a maximum.

The mean number of saddle points with an avoidance range less than or equal to z can also be computed,

$$\langle \tilde{\mathcal{I}}(z) \rangle = \frac{k^2 |\Omega|}{4\pi} \frac{3z^2(16 - z^2)^2}{(512 - 64z^2 + 3z^4)^{3/2}} \qquad 0 < z < 2\sqrt{2}. \tag{17}$$

The normalization gives trivially the mean number of saddle points in the ensemble. Therefore we can define the probability

$$\mathcal{I}_{r.w.}(z) = \frac{\langle \tilde{\mathcal{I}}(z) \rangle}{\langle N_S \rangle} = \frac{3\sqrt{3}z^2(16 - z^2)^2}{(512 - 64z^2 + 3z^4)^{3/2}} \qquad 0 < z < 2\sqrt{2} \tag{18}$$

with a corresponding density

$$\mathcal{P}_{r.w.}(z) = \frac{6144\sqrt{3}z(8 - z^2)(16 - z^2)}{(512 - 64z^2 + 3z^4)^{5/2}} \qquad 0 < z < 2\sqrt{2}. \tag{19}$$

These results served to test the conjecture that the bulk properties of the nodal sets of chaotic wavefunctions are reproduced by the predictions of the isotropic random wave ensemble. For this purpose we computed numerically the first 2400 eigenfunctions of the Sinai billiard shown in figure 1(*c*). For each wavefunction the critical points were found by a numerical search. The saddles which correspond to boundary intersections were excluded.
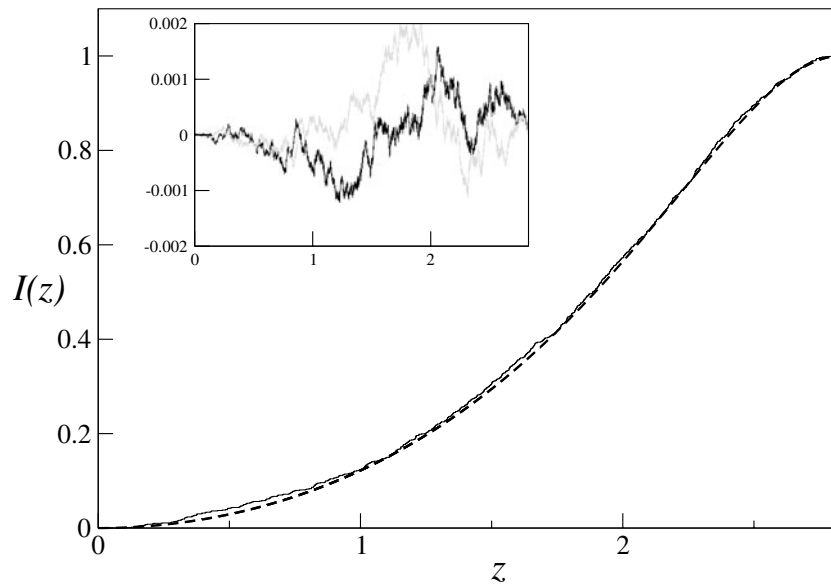
Figure 3. Counting function $\mathcal{I}(z)$ for the $n = 2000$ eigenstate of the Sinai type billiard (full thin line), compared with the random wave prediction (18) (dashed line). Inset: difference between the average counting function over the $n = (1800, 2000)$ eigenstates and the random wave prediction (dark line); the same for $n = (2200, 2400)$ eigenstates (light line).

The avoidance range (10) was computed for each saddle. In figure 3 we plot the cumulative histogram of the avoidance ranges for the 2000th eigenstate as full line (1102 saddle points), compared with formula (17) as dashed line. Even for a single eigenstate the agreement is very good. Averaging the avoidance range distributions over a group of neighbouring eigenstates the numerical histogram and the theoretical curve approximately coincide. The inset of figure 3 shows the differences between the random wave prediction and the mean avoidance range distributions computed for two groups of eigenstates. The difference is small, and shows no systematic deviations.

Another distribution which we compared to the prediction of the random wave ensemble is the number of saddle points. Normalizing the number of saddle points by the prediction of the isotropic random wave ensemble, we observe that as k increases the numerical computation approaches the predicted value (see figure 4).

The systematic deviation observed at finite k is due to boundary effects. Following [6] we compute the effect of an infinite straight Dirichlet line, which is reproduced by the wave ensemble

$$\Psi(\mathbf{r}) = 2 \sum_{n=1}^{\infty} c_n \sin(n\theta) J_n(kr) \tag{20}$$

where the c_n are real coefficients taken as independent random Gaussian distributed variables.

Not entering into the details of the calculation, the computed mean density of saddle points approaches the bulk expression (16) as the distance from the Dirichlet line increases. The integrated density in the perpendicular direction shows a global deficiency of saddle points relative to the bulk value. It diverges logarithmically as a function of the distance from the Dirichlet line [6].
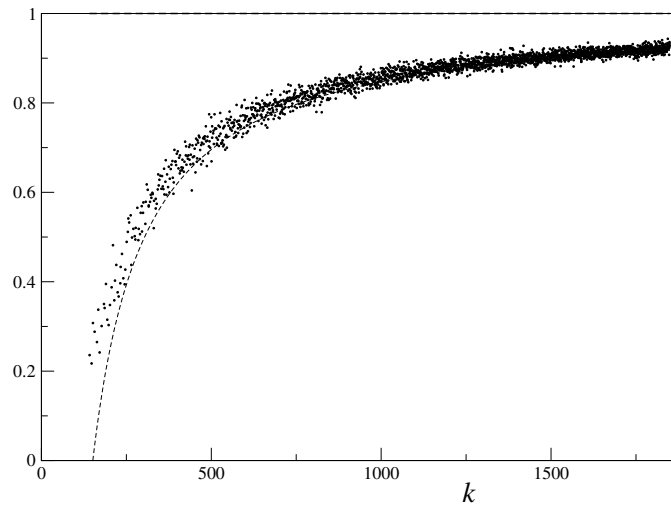
Figure 4. Number of saddle points for the first 2400 eigenstates of the Sinai billiard, normalized by the isotropic random wave prediction $k^2/(4\pi\sqrt{3})$, as a function of the wave number k. Dashed line: equation (21) for the anisotropic random wave ensemble (20).

We compared the results of the ensemble (20) to the number of saddle points counted for highly excited eigenstates of a chaotic billiard with sufficiently smooth boundaries. The integral along the boundary multiplies the density by the perimeter of the billiard $\mathcal{L}$. The perpendicular integral must be truncated in view of the logarithmic divergence mentioned above. A sensible choice of the truncation distance is $R = \sqrt{|\Omega|}/2$. The resulting estimate for the mean number of saddle points is

$$\langle N_S \rangle \approx \frac{k^2|\Omega| - k\mathcal{L}(\sigma_1 \log(kR) + \sigma_2)}{4\pi\sqrt{3}}. \tag{21}$$

with $\sigma_1 \approx 0.014$ and $\sigma_2 \approx 2.0$. The deficiency of saddle points is explained by the effect of the Dirichlet boundaries that affects the statistics. The dashed line in figure 4 represents equation (21) and the agreement is definitely improving. However, the domain of low values, $k < 500$, is not in complete agreement. This deficiency can be associated with the corners of the billiard, with its curvature or with the finiteness of the Dirichlet line that the ensemble (20) cannot reproduce. These possible causes will be studied elsewhere.

In conclusion, we can say that the properties of the nodal set of chaotic wavefunctions which were investigated in this work are very well reproduced by the isotropic random wave ensemble in the semiclassical domain. These findings are consistent with previous works on the subject, and add support to the random wave conjecture.

Acknowledgments

References

[1] Stratt R M, Handy N C and Miller W H 1979 *J. Chem. Phys.* **71** 3311–22
[2] Simmel F and Eckert M 1996 *Physica* D **97** 517
[3] Blum G, Gnutzmann S and Smilansky U 2002 *Phys. Rev. Lett.* **88** 114101
[4] Berry M V 1977 *J. Phys. A: Math. Gen.* **10** 2083–91
[5] Bogomolny E and Schmidt C 2002 *Phys. Rev. Lett.* **88** 114102
[6] Berry M V 2002 *J. Phys. A: Math. Gen.* **35** 3025–38
[7] Bies W E and Heller E J 2002 *J. Phys. A: Math. Gen.* **35** 5673–85
[8] Courant R and Hilbert D 1953 *Methods of Math. Phys.* vol I (New York: Interscience) pp 451–65
[9] Pleijel A 1956 *Commun. Pure Appl. Math.* **9** 543
[10] Krahn E 1924 *Math. Ann.* **94** 97–100
[11] Donnelly H and Fefferman C 1988 *Invent. Math.* **93** 161
Donnelly H and Fefferman C 1990 *J. AMS* **3** 333
Donnelly H and Fefferman C 1992 *J. Geom. Anal.* **2** 79
[12] Hoffmann-Osterhof T *et al* 1999 *Geom. Funct. Anal.* **9** 1169–80
[13] Uhlenbeck K 1976 *Am. J. Math.* **98** 1059
[14] Graf J H 1893 *Math. Ann.* **43** 142–4
See also Watson G N 1996 *A Treatise on the Theory of Bessel Functions* (Cambridge: Cambridge University Press) pp 359–61